Cross-tropopause transport of surface pollutants during the Beijing July 21 deep convection event

Xi Chen, Luolin Wu, Xiaoyang Chen, Yan Zhang, Jianping Guo, Sarah Safieddine, Fuxiang Huang, Xuemei Wang

Cross-Tropopause Transport of Surface Pollutants during the Beijing 21 July Deep Convection Event

XI CHEN,[a,b] LUOLIN WU,[c] XIAOYANG CHEN,[d] YAN ZHANG,[b] JIANPING GUO,[e] SARAH SAFIEDDINE,[f] FUXIANG HUANG,[b] AND XUEMEI WANG[g]

[a] *School of Environmental Science and Engineering, Sun Yat-Sen University, Guangzhou, China*
[b] *National Satellite Meteorological Center, Beijing, China*
[c] *School of Atmosphere Sciences, Sun Yat-Sen University, Zhuhai, China*
[d] *Department of Civil and Environmental Engineering, Northeastern University, Boston, Massachusetts*
[e] *State Key Laboratory of Severe Weather, Chinese Academy of Meteorological Sciences, Beijing, China*
[f] *LATMOS/IPSL, Sorbonne Université, UVSQ, CNRS, Paris, France*
[g] *Guangdong–Hong Kong–Macau Joint Laboratory of Collaborative Innovation for Environmental Quality, Institute for Environmental and Climate Research, Jinan University, Guangzhou, China*

(Manuscript received 28 April 2021, in final form 21 January 2022)

ABSTRACT: Air transport from the troposphere to the stratosphere plays an important role in altering the vertical distribution of pollutants in the upper troposphere and lower stratosphere (UTLS). On 21 July 2012, Beijing was hit by an unprecedented extreme rainfall event. In the present study, the Community Multiscale Air Quality Modeling System (CMAQ) is used to simulate the change in vertical profiles of pollutants during this event. The integrated process rate (IPR) method was applied to quantify the relative contributions from different atmospheric processes to the changes in the vertical profile of pollutants and to estimate the vertical transport flux across the tropopause. The results revealed that, in the tropopause layer, during the torrential rainfall event, the values of O_3 decreased by 35% and that of CO increased by 98%, while those of SO_2, NO_2, and $PM_{2.5}$ increased slightly. Atmospheric transport was the main cause for the change in O_3 values, contributing 32% of the net increase and 99% of the net decrease of O_3. The calculations showed that the transport masses of CO, O_3, $PM_{2.5}$, NO_2, and SO_2 to the stratosphere by this deep convection in 25 h were 6.0×10^7, 2.4×10^7, 7.9×10^5, 2.2×10^5, and 2.7×10^3 kg, respectively, within the ~300 km × 300 km domain. In the midlatitudes of the Northern Hemisphere, penetrating deep convective activities can transport boundary layer pollutants into the UTLS layer, which will have a significant impact on the climate of this layer.

KEYWORDS: Deep convection; Stratophere-troposphere coupling; Ozone

1. Introduction

The transport of tropospheric pollutants into the stratosphere increases their lifetime and results in the spread of pollutants on a global scale, in turn affecting the global radiation budget and climate (Randel et al. 2010; Solomon et al. 2011). The Asian summer monsoon circulation in the Northern Hemisphere (NH) is an important "window" for pollutant transport (Randel et al. 2010; Tang et al. 2011). Previous studies have shown that persistent maxima in CO, minima in O_3 (Park et al. 2007), and high values of SO_2 and aerosols (Yu et al. 2017; Vernier et al. 2011, 2015; Lamarque et al. 2012) within the anticyclone in the upper troposphere and lower stratosphere (UTLS) throughout summer. This is a result of the combined effects of deep convection and anticyclone caused by the Asian monsoon (Ploeger et al. 2017). Pollutants can be transported from the boundary layer to the upper troposphere within 30 min, or even less, due to strong updrafts. Then they are then captured by the large-scale uplifting anticyclone, and penetrate into the stratosphere (Dessler and Sherwood 2004; Lelieveld et al. 2018). For these reasons, the deep convection provides the power for air entering the stratosphere.

Penetrating deep convection can directly transport pollutants to the lower stratosphere with an occurrence probability of 0.5%–1.5% (Li et al. 2010). In the tropics, both slow ascent and rapid deep convection contribute to the composition and thermal structure of the tropical tropopause layer (Randel and Jensen 2013). Liu and Zipser (2005) observed that 0.1% of tropical convection systems may even penetrate the 380 K potential temperature level (top of the lowermost stratosphere). Although thunderstorms constitute a major forcing in the convective overturning of the troposphere, particularly in the tropics, synoptic disturbances such as extratropical cyclones also cause rapid vertical mixing (Lelieveld and Crutzen 1994). In the northern middle to high latitudes, the convection penetrating the tropopause is as frequent as those over the tropics (Liu and Liu 2016). In addition, the heights of the tropopause in the middle latitudes of the NH are lower than those in the tropical regions. After entering the lower stratosphere, the pollutants will affect the global pollution distribution and lifetime through isentropic transportation (Doherty et al. 2005).

Supplemental information related to this paper is available at the Journals Online website: https://doi.org/10.1175/JAS-D-21-0115.s1.

Corresponding author: Xuemei Wang, eciwxm@jnu.edu.cn; Fuxiang Huang, huangfx@cma.cn

DOI: 10.1175/JAS-D-21-0115.1

The influence of deep convection on global climate must not be ignored. With the increase of the equatorial updraft from 1984 to 2009, there has been a 3% decade^{-1} decrease in O_3 value in the tropical lower stratosphere, resulting in a drop in global temperature (Randel and Jensen 2013). Cross-tropopause transport significantly affects the global aerosol distribution (Yu et al. 2017). Near-global satellite aerosol data imply a negative radiative forcing due to stratospheric aerosol changes over this period of about -0.1 W m^{-2}, thereby reducing the global warming that would otherwise have occurred in recent years (Solomon et al. 2011). Both physical and chemical processes caused by deep convection can affect the values of pollutants; for example, changes in O_3 values, which depend on the NO_x generated by lightning and its relationship with volatile organic compounds (VOCs), are related to processes within the cloud (Khodayari et al. 2018; Liaskos et al. 2015).

Quantifying the exchange of ozone between the stratosphere and troposphere is important due to their key roles as greenhouse gases and chemically active species in the UTLS (Gettelman et al. 1997; Büker et al. 2008; Hsu et al. 2005; Hitchman et al. 2004; Tang et al. 2011; Li et al. 2005). Tang et al. (2011) calculated the stratosphere–troposphere exchange of ozone using chemical transport models, and the results indicated that, during June, 49% of the ozone fluxes in the NH are related to deep convection. Li et al. (2005) observed that deep convective outflow in the boundary layer accounts for about 30% of the total export of North American CO. However, only a small number of studies have analyzed the process of pollutant change and quantified the cross-tropopause transport flux in the deep convection. This study will analyze the vertical changes of pollutants in view of the penetrating deep convection event that occurred in Beijing, and apply atmospheric chemistry models to quantify the effects of different processes on concentration changes, then finally calculate the vertical transport flux of pollutants.

During an event which occurred on 21 July 2012, Beijing and its surrounding areas suffered the strongest rainstorm and flood disaster in 61 years, resulting in many casualties and widespread property damage. This intense torrential rain produced an enormous updraft and formed a penetrating deep convection system, in turn resulting in the transport of surface pollutants to the stratosphere. Beijing, due to its high population density and rapid growth, has been affected with severe levels of tropospheric O_3 and $PM_{2.5}$ (Lu et al. 2018; Wang et al. 2011; Chen et al. 2018). This provides a unique opportunity to study the effects that the physical and chemical processes occurring within this deep convective system have on the vertical profiles of these and other pollutants.

This study used Community Multiscale Air Quality (CMAQ), version 5.1, coupled with Weather Research and Forecasting (WRF) Model, version 3.7, to simulate the Beijing 21 July torrential rainfall event. The main scientific questions posed were as follows:

1) What were the changes in the vertical profiles of pollutants during this deep convection event?
2) What were the contributions of gas-phase chemical processes, source emissions, horizontal and vertical transport, dry deposition, aerosol processes, and cloud processes to the pollutant changes?
3) What masses of the pollutants were transported to the stratosphere during this deep convective event?

To address these questions, O_3 was selected as the pollutant to analyze the vertical profile change and contributions of different processes (sections 3a and 3b). The model results were then used to calculate the cross-tropopause transport fluxes of O_3, CO, SO_2, NO_2, and $PM_{2.5}$ (section 3c). Finally, satellite data were used to analyze the intensity and distribution of global deep convection, so as to compare the potential of cross-tropopause transport on a global scale (section 3d).

2. Data and methods

a. Data

This study drew from four different datasets. The first is the ERA-Interim dataset provided by the European Centre for Medium-Range Weather Forecasts (ECMWF). ERA-Interim is a global atmospheric reanalysis based on a data assimilation system (Dee et al. 2011). It is available for the period from 1 January 1979 to 31 August 2019. The data used in this study include the relative humidity (unit: %), U and V components of the wind (unit: m s^{-1}), vertical velocity (unit: Pa s^{-1}), and ozone mass mixing ratio (unit: kg kg^{-1}) from 1 to 31 July 2012. The vertical height was divided into 37 layers from 1000 to 1 hPa, the latitude and longitude ranges were 30°–50°N and 105°–130°E, respectively, and the spatial resolution was 0.25° × 0.25° (https://www.ecmwf.int/en/forecasts/datasets/archive-datasets/reanalysis-datasets/era-interim). The ozone mass mixing ratio is the mass of ozone per kg of air. In the ECMWF Integrated Forecasting System (IFS), there is a simplified representation of ozone chemistry (including tropospheric chemistry and stratospheric chemistry) (Wedi et al. 2015). Most of the IFS chemical species are archived as mass mixing ratios (kg kg^{-1}). The ERA-Interim dataset was used to verify the meteorological field simulation of the WRF/CMAQ model, and to analyze the vertical profile change of O_3. The second is the NCEP reanalysis data from the National Oceanic and Atmospheric Administration (NOAA). The NCEP–NCAR Reanalysis 1 project employs a state-of-the-art analysis/forecast system to perform data assimilation using data from 1948 to the present. It provides climate datasets on multiple time scales worldwide with a spatial resolution of 2.5° × 2.5°. The tropopause level data at 6 h intervals have also been used by many researchers (e.g., Liu and Zipser 2005) to analyze the tropopause changes during deep convection (https://www.esrl.noaa.gov/psd/data/gridded/data.ncep.reanalysis.html). The third is the L-band sounding data from the China Meteorological Administration (CMA) (Guo et al. 2016). The GTS1 digital electronic radiosonde, one of the key components of the L-band sounding system, is now widely used at operational radiosonde stations throughout China, providing fine-resolution profiles of temperature, pressure, relative humidity, wind speed, and direction twice a day, at 0000 UTC (0800 BJT) and 1200 UTC (2000 BJT), for detection heights of up to 40 km. The vertical wind speed and temperature data from the Beijing Observatory (39.8°N, 116°E) were used to verify the vertical

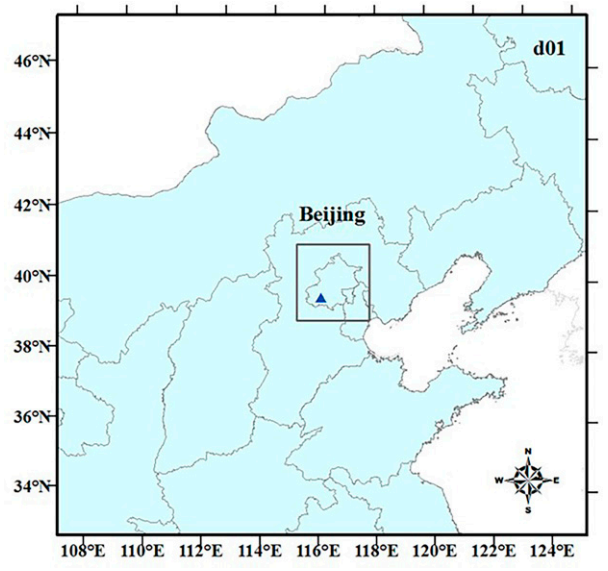

FIG. 1. Study area in WRF/CMAQ. The box denotes the Beijing area (39°–41°N, 115°–118°E). The blue triangle indicates the meteorological sounding station and its location in Beijing.

simulation accuracy of the model. The fourth is the global surface pollutant concentrations originating from the Modern-Era Retrospective Analysis for Research and Applications, version 2 (MERRA-2). The extracted monthly mean aerosol diagnostic fields and CO concentrations had a spatial resolution of 0.5° × 0.625° (https://disc.gsfc.nasa.gov/datasets/M2TMNXAER_5.12.4/summary).

b. Methods

The model used in this study is the WRF/CMAQ (offline). Large-scale meteorological fields and boundary conditions were adopted in conjunction with the global 6 h interval FNL forecast data provided by NCEP. The simulation area is shown in Fig. 1. The model applied LAMBERT projection with a center point of 40°N, 116.4°E. The horizontal grid resolution was 27 km, the number of grids was 100 × 100, and the terrain followed the coordinates in the vertical direction. There were 39 layers in total, with the pressure at the model top being 50 hPa. The simulation time period was from 18 to 24 July 2012, and the simulation was initiated 3 days in advance to include the initialization process and reduce the influence of the initial conditions.

In the present study, O_3 was used as a model pollutant to analyze the effects of atmospheric processes on the pollutants' value in deep convection events by using integrated process rate (IPR) analysis. The IPR analysis in CMAQ can be used to calculate the influence of different atmospheric processes on the values of pollutants, and to quantify the importance of each process in the evolution of the pollutant value. Mathematically, it can be expressed as follows (Byun and Ching 1999):

$$c(t + \Delta t) = c(t) + \sum_{n=1}^{N} (\Delta C)_n, \tag{1}$$

$$(\Delta c)_n = \int_t^{t+\Delta t} L_n dt, \tag{2}$$

where c is the species concentration, Δc is the concentration change of a species due to operator n (IPRn), Δt is the model synchronization time step used by the chemical solver, and L_1 to L_n represent the differential operators associated with the processes. In this study, the processes include gas-phase chemistry, source emissions, horizontal transport, vertical transport, dry deposition, aerosol processes, and cloud processes. Specifically, the emission sources include anthropogenic, biogenic, fire, wind-blown dust, and sea spray emissions. Horizontal transport includes horizontal advection and diffusion, while vertical transport includes convection and diffusion. In addition, aerosol processes treated within the CMAQ aerosol component include new particle formation, intermodal and intramodal coagulation, and particle growth by addition of mass. The aerosol module uses differential equations to represent conservation of particle number, surface area, and species mass for each mode, then solves these equations analytically (Mebust et al. 2003). Clouds affect the trace atmospheric species through a number of physical and chemical processes, including the following: 1) vertical transport (convective updrafts and downdrafts); 2) scavenging of atmospheric aerosols and gases, and subsequent chemical reactions leading to the formation of secondary species; 3) wet deposition (removal from the atmosphere through rainout or washout); and 4) altering radiative transfer and optics.

The atmospheric process can be divided into two categories depending on their effect on O_3 value: 1) processes increasing the O_3 value, corresponding to IPR > 0, termed net increase processes; 2) processes reducing the O_3 value, corresponding to IPR < 0, known as net reduction processes (Liu et al. 2012). The importance of a particular atmospheric process in the overall net increase or net reduction process can be calculated by the following formula:

$$N\_\text{increase}_{(n)} = \frac{\sum_t \text{IPR}_{n,t}}{\sum_p \left(\sum_t \text{IPR}_{n,t} \right)} \times 100\% \ (\text{IPR}_{n,t} > 0), \tag{3}$$

$$N\_\text{reduction}_{(n)} = \frac{\sum_t \text{IPR}_{n,t}}{\sum_p \left(\sum_t \text{IPR}_{n,t} \right)} \times 100\% \ (\text{IPR}_{n,t} < 0), \tag{4}$$

where n is the process, t is time, and N_increase_n and $N\_\text{reduction}_n$ are the net increase ratio and net reduction ratio, which respectively indicate the proportion of the atmospheric phenomena in the net increase and net reduction processes, thereby reflecting their relative importance to the change in O_3 values. Next, IPR process analysis can be used to calculate the balance of each species on unit grid, and to quantify its value changes as the contribution of different processes. To perform the quantitative analysis of the cross-tropopause transport of polluted compositions, the integral of

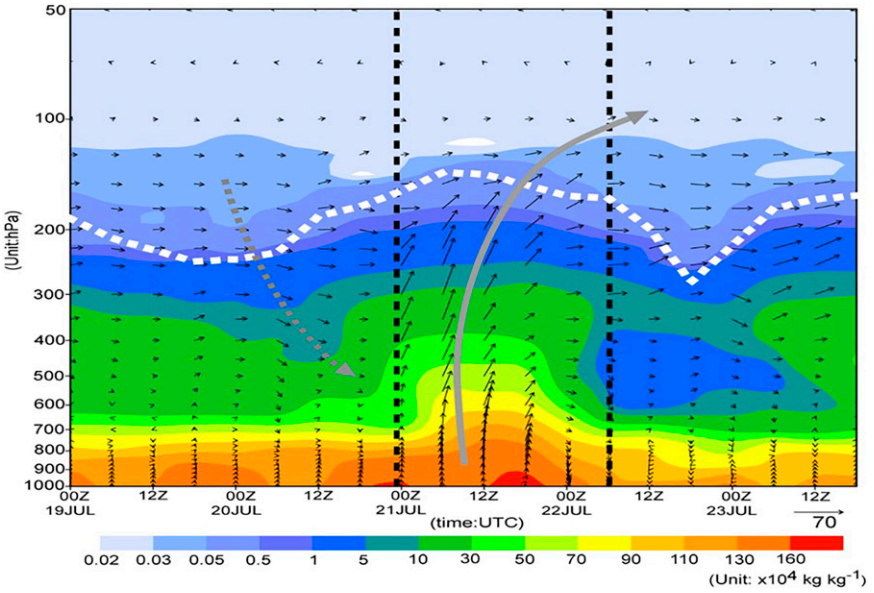

FIG. 2. Time series of regional mean atmospheric humidity vertical distribution (color shaded), vertical U–W wind fields (black vectors, component W/500, in m s^{-1}), and tropopause height (white thick dashed line) averaged over the study area of 39°–41°N, 115°–118°E from 0000 UTC 19 Jul to 1800 UTC 23 Jul 2012. The black dashed lines define the severe rainfall period, and the gray dashed (solid) curve indicates the airstream coming from the upper (lower)-level troposphere to the lower (upper)-level troposphere. Data source: ERA-Interim and NCEP.

the IPR (process: vertical transport) from the tropopause (defined by the NCEP–NCAR reanalysis dataset) to the top of the model was calculated. The formula for calculating the transport flux per hour (unit: kg km^{-2} h^{-1}) is as follows:

$$\text{Transport flux} = \sum_{j=\text{tropopause}}^{\text{model top}} \text{IPR}_{v,j} \times Z_j, \qquad (5)$$

where $\text{IPR}_{v,j}$ indicates the IPR value corresponding to vertical transport on the j layer, i.e., the change in the values of pollutants caused by the vertical transport (unit: kg km^{-3}); and Z is the height of each layer (unit: km).

3. Results

a. Simulation of deep convection events

During the extreme deep convection event, the torrential rainfall began in the Beijing area at approximately 0000 UTC 21 July and ended at around 0600 UTC 22 July. Beijing and the surrounding regions were controlled by the influence of deep convection motion with favorable moisture conditions associated with southeast flow, which caused an abrupt increase in precipitation. At 1200 UTC, a low-level convergence generated by the northwest vortex resulted in a strong upper-level divergence and enhanced vertical motion leading to the largest hourly precipitation at 1300 UTC. During this episode (Fig. 2), tropospheric air infiltrated into the stratosphere, accompanied by a rapid increase in water vapor at the surface. Under the influence of the change of atmospheric temperature gradient caused by latent heat heating, adiabatic rise of air, and change in total ozone (Gettelman and Birner 2007; Tian et al. 2008), the height of the tropopause rose from 240 to 175 hPa (~13 km). Taking into account the vertical resolution of the model, the average tropopause height of 175 hPa (~13 km) was used for subsequent analysis (Duncan et al. 2007).

1) SIMULATION OF THE METEOROLOGICAL FIELD

In this study, first the WRF Model was run to obtain the required meteorological input fields for the CMAQ model. The comparison results of temperatures and wind speeds from the model simulation and L-band sounding observation in the Beijing area are shown in the online supplemental material. Both sets of data passed the t test, and the results showed no significant differences (significance level = 0.01), thus leading to the conclusion that the WRF Model can be used to accurately simulate temperature and wind speed. In addition to the sounding data, we used ERA-Interim data from the ECMWF for wind fields and relative humidity verification. The height–longitude cross section at 40°N is shown in Fig. 3. From the perspective of relative humidity distribution and wind speed, the meteorological elements of the WRF simulation were shown to be consistent with the ECMWF products.

Deep convection activities undergo a process of development and displacement. Comparing Figs. 3a–c, from 20 to 22 July, the intensity of deep convection gradually increased. The height that could be reached by the updraft caused by deep convection also increased, from 180 to 130 hPa. On 20 July, the updraft occurred west of 110°E, and the intensity

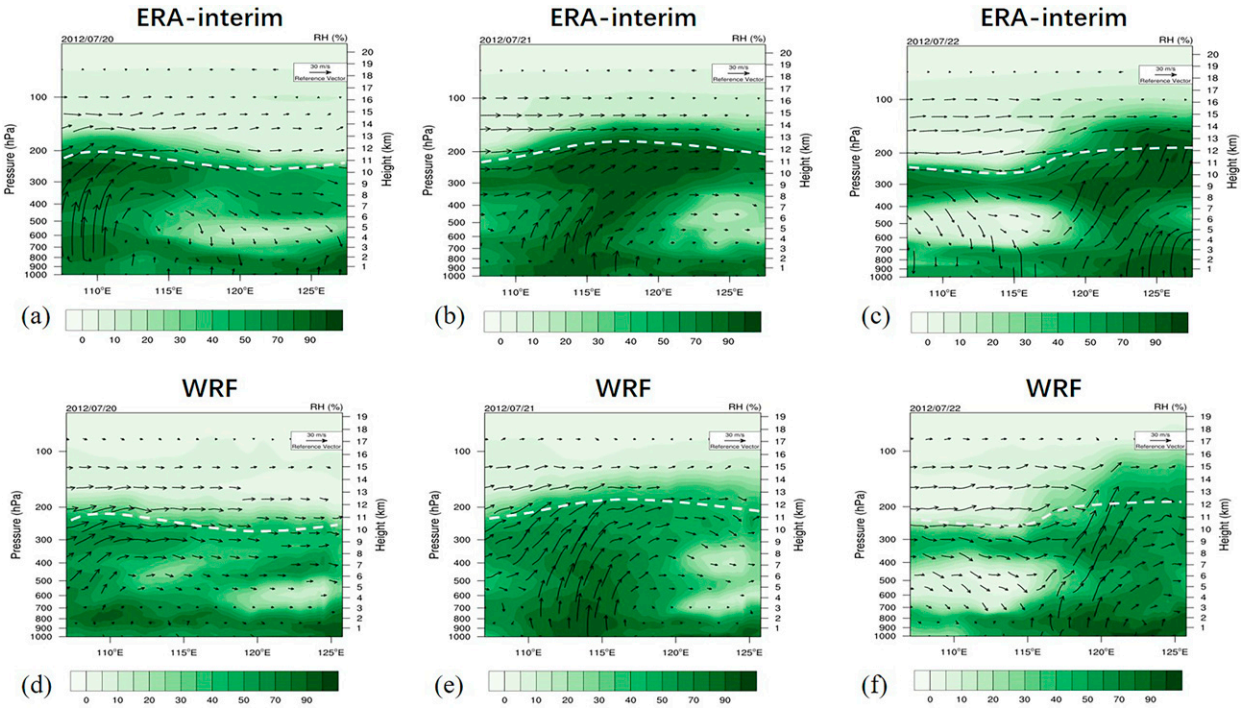

FIG. 3. Comparison of relative humidity in height–longitude section and the vertical wind fields for 20–22 Jul 2012. Rows show results from (a)–(c) ECMWF data and (d)–(f) the WRF simulations. The white dashed lines represents the tropopause height from NCEP.

of convection was low, leading to sinking motion over Beijing (116.4°E). On 21 July, the deep convection activity increased and moved between 110° and 115°E. Due to the westerly winds, when the airflow rose to the top of the troposphere, the center shifted eastward to 115°–120°E. On 22 July, the deep convection center exited the Beijing area and continued to develop eastward, with its intensity gradually increasing. During these three days, the area underwent different levels of tropospheric uplift and water vapor transport to the lower stratosphere, with the most significant transport occurring on 22 July. At the same time, in the draft region, relative humidity decreased, which was caused by the low value of water vapor in the stratosphere entering the troposphere (Holton et al. 1995).

2) SIMULATION OF O_3

Deep convection can transport pollutants from the boundary layer to the stratosphere, in turn affecting the content of water vapor and pollutants in the stratosphere (Park et al. 2004, 2007). Previous studies have shown that in summertime convection over the NH, the mesoscale ageostrophic movements and tropopause deformation around the convective region result in STE and ozone enhancement in the free troposphere (Tang et al. 2011). For the deep convection episode, changes in the vertical distribution of O_3 were compared with ECMWF and WRF-CMAQ simulation output (Fig. 4). The ozone value and wind fields change of ECMWF and CMAQ are basically the same above 700 hPa; however, there is a difference in ozone distribution between ECMWF and CMAQ below 700 hPa. ECMWF does not simulate the daily change of ozone, yet the ozone value near the ground simulated by CMAQ varies from 9 to 141 ppb, with an average of 60.7 ppb. The change in ozone distributions indicate that the updraft carried low values of ozone into the stratosphere on 21 July, thereby causing the stratospheric ozone value to decrease significantly. Due to the departure of the rainstorm center and the intrusion of the sinking air, on 22 July the vertical wind direction changed from upward to downward. The ozone that was raised to the upper level began to fall, and finally a high value area of ozone was formed near 485 hPa. In terms of surface ozone, since 1200 UTC 21 July, the values of surface ozone began to decrease, from 100 to 40 ppb, and its low value continued until after 22 July before it began to gradually recover.

To analyze the transport of ozone by deep convection, a distribution chart of O_3 value with a cross section of 175 hPa is presented in Fig. 5. Before the occurrence of the deep convection, the O_3 value over Beijing ranged between 130 and 150 ppb, decreasing to 80–100 ppb during the convection period, then returning to 130–150 ppb when the convection center exited the area. This indicates that, during the rainfall period on 21 July, the average O_3 value in the Beijing area dropped almost 35%, i.e., by 47 ppb.

b. Factors affecting the vertical profile O_3

The impact of deep convective activities on ozone is mainly reflected in terms of two aspects: the transport of ozone itself and the transport of ozone precursors. It is understandable

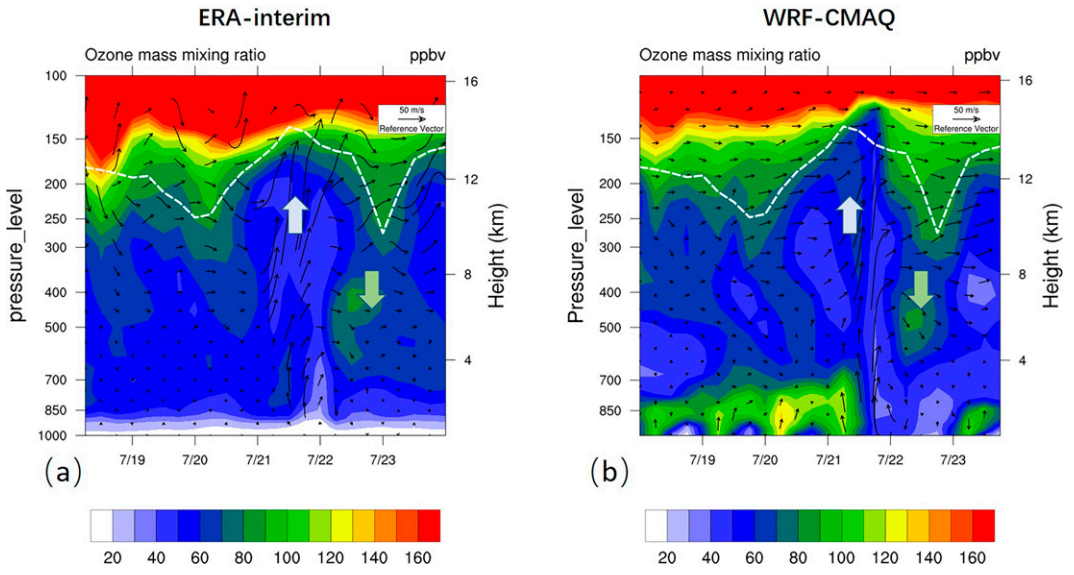

FIG. 4. Time series of regional mean ozone mixing ratio vertical distribution (color shaded), vertical U–W wind fields (black vectors, component W/300, in m s^{-1}), and tropopause height (white thick dashed line) averaged over the study area of 39°–41°N, 115°–118°E from 0000 UTC 18 Jul to 1800 UTC 24 Jul 2012.

that the transport processes are accompanied by the impact of different atmospheric processes on ozone. To explore the processes which affected the vertical profile of O_3, the IPR method in CMAQ was used to quantify the relative contributions from vertical transport (VTRA; including vertical advection and diffusion), horizontal transport (HTRA; includes horizontal advection and diffusion), emission (EMIS), dry deposition processes (DDEP), cloud processes (CLDS), chemical processes (CHEM), and aerosol processes (AERO). Figure 6 presents the respective effects of different processes on change in O_3 values at representative altitudes of 0.6, 6, and 13 km for the lower-, middle-, and upper-tropospheric regions.

At 13 km (Fig. 6a), the respective daily average O_3 values from the 20 to 22 July were 133, 86, and 131 ppb. The changes in O_3 values were characterized by low values during rainfall. On 21 July, the vertical transport had a positive contribution while horizontal transport exhibited a negative contribution, and the net contribution of the atmospheric transport was −70 ppb. At 6 km (Fig. 6b), the respective daily average O_3 values were 88, 67, and 93 ppb. The change in O_3 values was characterized by a decrease during the rainfall and an increase thereafter, which was mainly related to atmospheric transport and cloud processes. Atmospheric transport had a negative contribution (−56 ppb), while in-cloud transportation had a positive one (35 ppb). At 0.6 km (Fig. 6c), the respective daily average O_3 values were 150, 121, and 57 ppb. The change in O_3 values was characterized by a decrease in the peak value at the beginning of the rainfall and a persistent low value after the rainfall. A number of factors may have been responsible for this decrease in O_3 value, with chemical processes playing a key role.

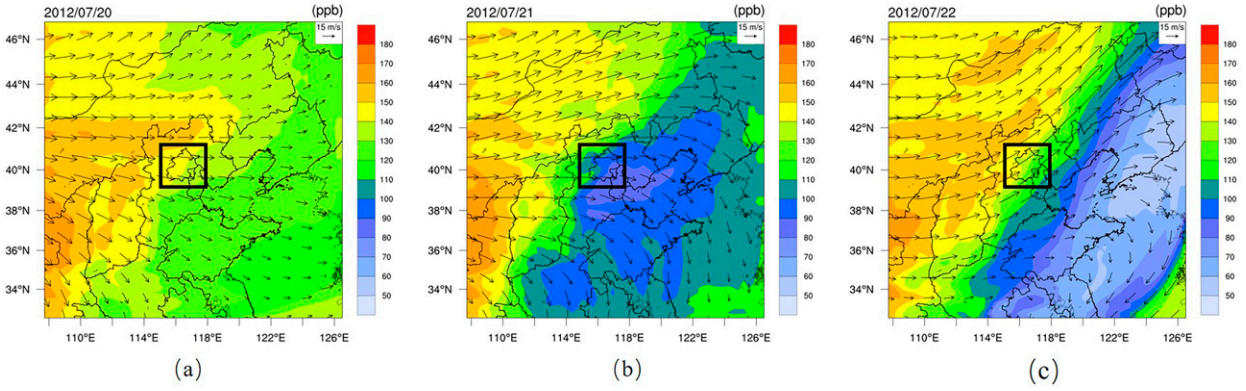

FIG. 5. WRF/CMAQ simulated O_3 value and wind fields at 175 hPa for (a) 20, (b) 21, and (c) 22 Jul. The black squares indicate the Beijing area.

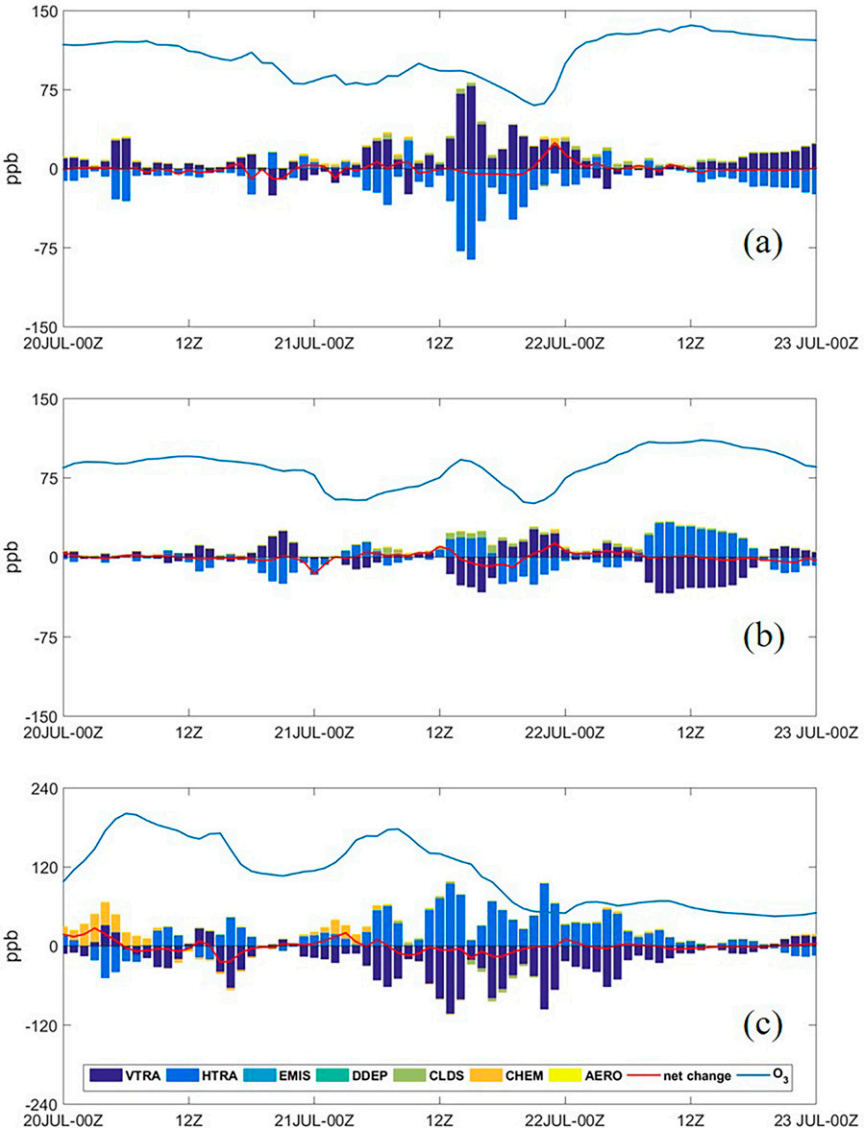

FIG. 6. Process analysis and O_3 time series of Beijing at (a) 13, (b) 6, and (c) 0.6 km. The blue curves are model simulated O_3, and the red curves are the total contributions of the seven processes. The color bars represent the different factors' contributions to increasing (positive) and decreasing (negative) O_3.

Figure 7 shows the vertical change of ozone value during deep convection and the contribution of atmospheric transport (combined vertical transport and horizontal transport) processes, chemical processes, and cloud processes mentioned above. In Fig. 7a, the change of ozone was divided into three typical regimes: Regime 1 was from 1500 to 2300 UTC 21 July, the height of which was 0–15 km. In this regime, low-value ozone spread to the entire troposphere and penetrated the tropopause to the stratosphere. Regime 2 was from 0100 to 2300 UTC 22 July, and the altitude was 0–2.5 km. There were persistently low levels of ozone in this regime. Regime 3 was from 0200 to 1800 UTC 22 July, and the altitude was 3.5–13 km. A high value of ozone appeared in this regime. During this episode, atmospheric transport was the most important factor affecting ozone changes, followed by chemical processes and cloud processes. Figure 7b shows the influence of atmospheric transport on the vertical distribution of ozone. The contribution of atmospheric transport to ozone varied with time, and the impact range is approximately ±20 ppb. Comparing the changes in the contribution of atmospheric transport from 21 to 22 July, we can clearly distinguish the influence of the updraft and downdraft on the ozone value. Atmospheric transport had a negative contribution to ozone in regimes 1 and 2, and a positive contribution to regime 3. Figure 7c shows the effect of chemical processes on the vertical distribution of ozone. It was not only related to the

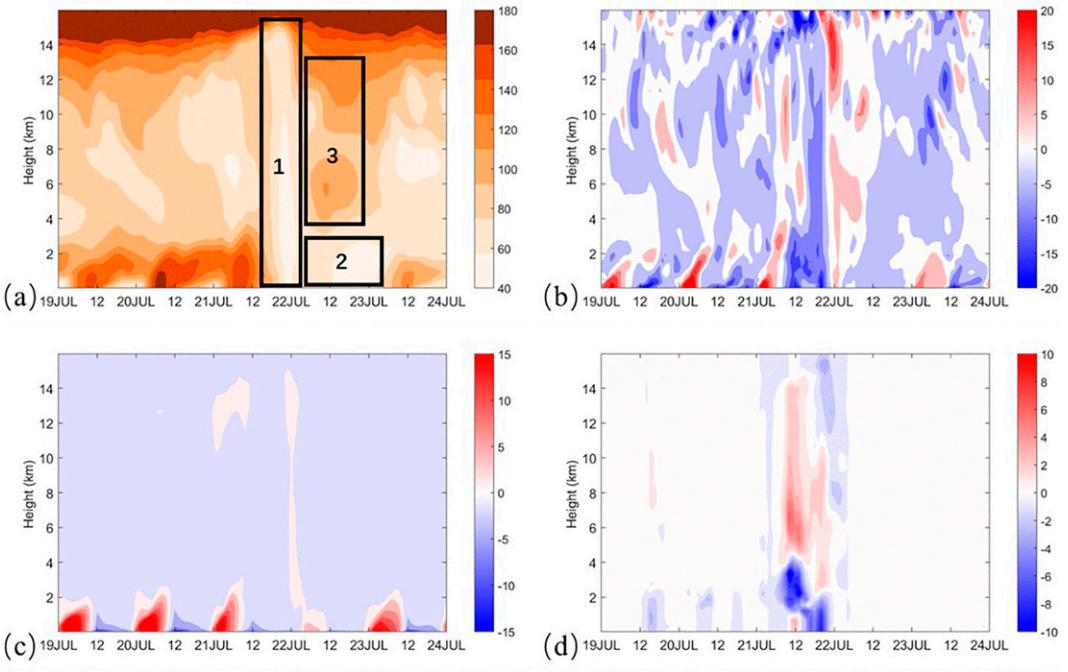

FIG. 7. Time–altitude changes of O_3 value and contributions of different processes thereto: (a) O_3 value, (b) atmospheric transport contribution, (c) chemical process contribution, and (d) cloud process contribution.

production of surface ozone, but also had an impact on upper-layer ozone due to the vertical transport in the atmosphere, and the impact on ozone was within ±10 ppb. Due to the removal of pollutants by heavy rains, the soluble ozone precursors decreased after 1200 UTC 21 July, which led to a significant reduction in the amount of ozone being produced after the rain. This process may have been the cause of the continued low ozone level in regime 2. While ozone precursors were greatly reduced due to the removal by rainfall, some precursors were still transported to high altitudes, where photochemical reactions occurred, thereby increasing the O_3 value (Doherty et al. 2005). Figure 7d illustrates the effect of cloud processes on the vertical distribution of ozone. Cloud processes include transport processes and chemical processes within the cloud. In the boundary layer, the cloud processes mainly resulted in the dry deposition of O_3, thereby reducing the ozone value (Hou et al. 2015; Zhao et al. 2010). In the middle and upper layers (200–400 hPa), the O_3 value in the cloud increased, due to the in-cloud transportation.

Based on the hourly IPR results from 20 to 22 July, the relative contribution of various atmospheric processes on the change in O_3 values in the lower (0.6 km), middle (6 km), and upper (13 km) troposphere were calculated, which are represented in Table 1. In the lower troposphere, the greatest net increase of O_3 was chemical processes (73%), followed by cloud processes (17%). In addition, atmospheric transport (83%) and chemical processes (10%) were the main removal mechanisms for O_3. In the middle troposphere, cloud processes and atmospheric transport became more prominent, respectively accounting for 64% and 32% of the O_3 production. The net reduction processes of O_3 were dominated by atmospheric transport (99%). In the upper troposphere, the production of O_3 was affected by cloud processes, atmospheric transport, and chemical processes, respectively accounting for 50%, 32%, and 19%. The removal of O_3 was still dominated by atmospheric transport, similar to the middle layer. In summary, chemical processes were the main cause of the net increase of low-level O_3 in this deep convection event, and the photochemical reaction between ozone precursors was responsible for the formation of ozone. Cloud processes were the main net increase of middle- and high-level O_3, while atmospheric transport was the critical cause for O_3 reduction over the entire altitude range. Under the influence of deep convection, the ozone generated near the surface can be transported to higher altitudes more quickly (Thompson 1994). The ascending motion induced by deep

TABLE 1. Effect ratio of atmospheric processes on change in O_3 values in the lower, middle, and upper troposphere. CHEM: chemical reactions; CLDS: cloud convections; ATRA: atmospheric transport. The boldface font indicates the greatest effect ratio among the atmospheric processes.

	Net increase (%)			Net reduction (%)		
Height (km)	CHEM	CLDS	ATRA	CHEM	CLDS	ATRA
0.6	**73**	17	10	10	7	**83**
6	5	**64**	32	1	0	**99**
13	19	**50**	32	0	1	**99**

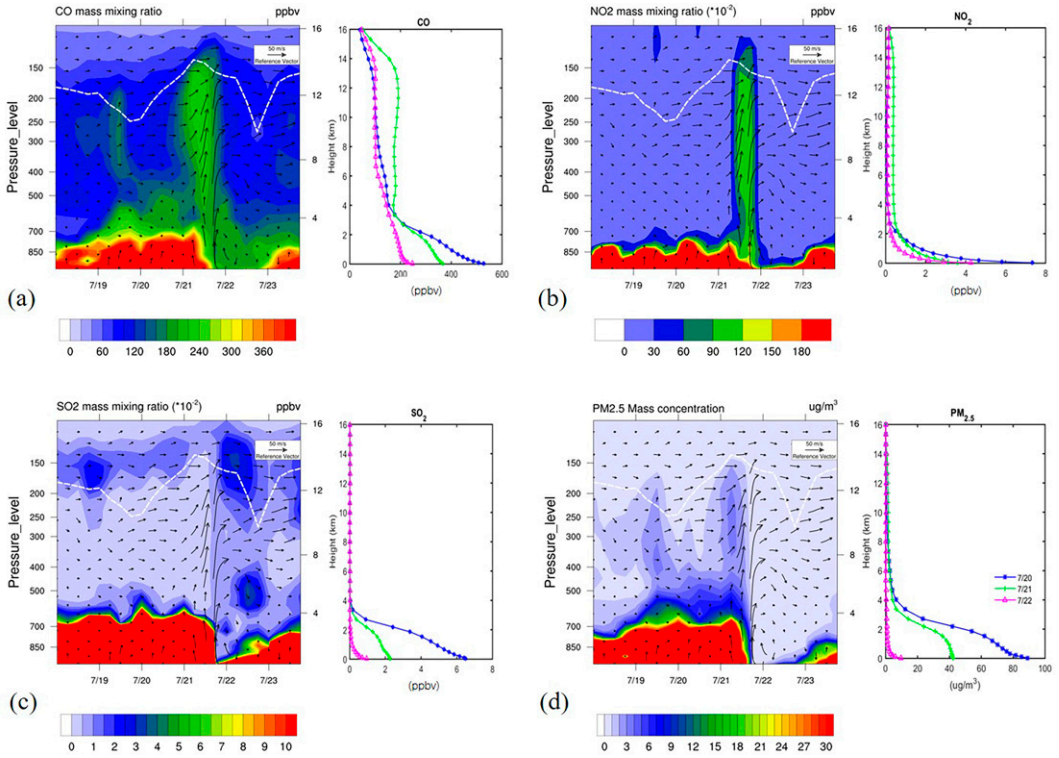

FIG. 8. As in Fig. 4, but for (a) CO, (b) NO_2, (c) SO_2, and (d) $PM_{2.5}$ as well as the daily average vertical profiles of each of the pollutants. Blue line: 20 Jul; green line: 21 Jul; red line: 22 Jul.

convection carries tropospheric ozone up to the stratosphere, where the O_3 lifetime is longer. This transport causes a decrease of O_3 in the upper troposphere, and at the same time the subsidence in the cloud environment carries O_3 of stratospheric origin downward from the upper troposphere into a regime in which the O_3 lifetime is shorter. This is only partly compensated by an increase in the lower atmosphere, eventually leading to a reduction in the total ozone column (Lelieveld and Crutzen 1994).

c. *Transport fluxes of pollutants*

Figure 8 shows the vertical profile changes of CO, NO_2, SO_2, and $PM_{2.5}$. During the deep convection, the values of CO significantly increased below the stratosphere, while the value changes of NO_2, SO_2, and $PM_{2.5}$ mainly occurred below 4 km, with small changes at high levels. Deep convection transported the high value of CO near the surface upward, resulting in a 98% (~120 ppb) of value increase at 13 km. The net increase in CO was mainly due to vertical transportation (44%) and cloud processes (55%) (Table S1 in the online supplemental material). At the same time, the values of NO_2, SO_2, and $PM_{2.5}$ were 1.25 ppb, 0.025 ppb, and 4.2 μg m^{-3}, respectively, which accounted for 9.5%, 0.13%, and 2.3% of the surface concentrations. This was because wet scavenging removed much of the SO_2 and $PM_{2.5}$ resulting in weak convective transport of these two species. The results of the process analysis also reveal that the net removal effect of the cloud process on SO_2 and $PM_{2.5}$ was greater than those of CO and NO_2 (Table S1). For relatively insoluble CO and NO_2 (Sander 2015), the NO_2 vertical transport appears to have been weaker than that of CO, mainly due to the fact that the NO_2 in the boundary layer air was reduced by washout, which then affected the mass of the NO_2 being transported to the free troposphere (Fig. S3a) (Yoo et al. 2014). In addition, the background concentration of CO in the troposphere was higher than that of NO_2. During the time periods before and after the formation of penetrating deep convection, weaker updrafts appeared in the middle troposphere, which could increase the vertical transport mass of CO (Fig. S3b). At the same time, deep convection led to an increase of NO_2, which attributed to cloud processes. These NO_2 will generate ozone through chemical reactions in the upper and middle troposphere (Fig. 7c).

As mentioned above, Eq. (5) indicates that the transport flux depends on the IPR value of vertical transport processes above the troposphere. Figure 9 analyzes the cross-tropopause transport fluxes of different pollutants. From 0000 to 2300 UTC 21 July, all five pollutants were transported from the troposphere to the stratosphere, and the values of transport flux at this time were positive. From 0000 to 2300 UTC 22 July, the direction of vertical transport altered, the intrusion of stratospheric air into the troposphere occurred, and the values of transport flux at this time were negative. For ozone, the deep convection activity was most vigorous between 1400 and 2000 UTC 21 July, and the velocity and cross-sectional

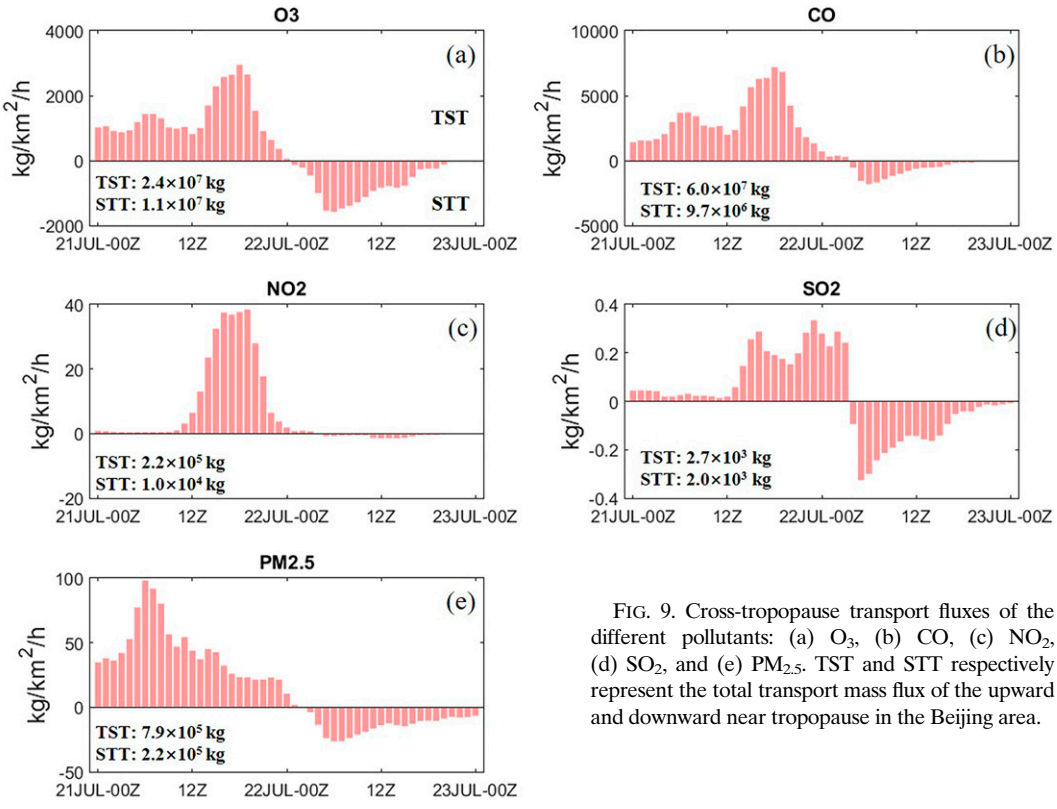

FIG. 9. Cross-tropopause transport fluxes of the different pollutants: (a) O_3, (b) CO, (c) NO_2, (d) SO_2, and (e) $PM_{2.5}$. TST and STT respectively represent the total transport mass flux of the upward and downward near tropopause in the Beijing area.

area of the updraft were the greatest. Therefore, although the O_3 value decreased, its transport flux increased significantly during this period. The highest value occurred at 1800 UTC 21 July, which was 2.94×10^3 kg km^{-2} h^{-1} (Fig. 9a). For CO, atmospheric transport transferred high-level CO in the lower layer to the tropopause, causing its value to increase. At 1800 UTC 21 July, the transport flux reached a maximum of 7.19×10^3 kg km^{-2} h^{-1} (Fig. 9b). For NO_2, the value of NO_2 was less than 0.1 ppb, which increased to 1.25 ppb, due to the influence of chemical processes, cloud processes and atmospheric transport. At 1900 UTC 21 July, the transport flux reached a maximum of 38.46 kg km^{-2} h^{-1} (Fig. 9c). For SO_2, its value of SO_2 was approximately 0.01 ppb in the upper layer, which also changed with deep convection activities: the effect of horizontal transport increased the value to 0.025 ppb, and the transport flux reached a maximum of 0.33 kg km^{-2} h^{-1} at 2300 UTC 21 July (Fig. 9d). For $PM_{2.5}$, its value in the upper layer ranged from 0.3 to 4.5 μg m^{-3} during the study period between 21 and 22 July. Under the effect of vertical transport, the transport flux increased with a maximum of 98.27 kg km^{-2} h^{-1} occurring at 0600 UTC 21 July (Fig. 9e). Comparing the changes in pollutant transport fluxes, those higher values of pollutants (such as O_3 and CO) were greatly affected by atmospheric transport. Therefore, the changes in the transport fluxes were consistent with the changes in the intensity of the updraft. For pollutants with strong wet scavenging rates (e.g., $PM_{2.5}$ and SO_2), their values are lowest at the time of the strongest convection, thus the timing of the maximum transport flux does not correspond to that of the maximum convection. In this deep convection event, the troposphere-to-stratosphere transport (TST) of pollutants was greater than the stratosphere-to-troposphere transport (STT). These differences also vary with different pollutants. For those boundary layer pollutants with low original concentration in the stratosphere, including CO, NO_2, and $PM_{2.5}$, the STT accounts for less than 30% of TST. After the pollutants have been transported to a higher layer, they continue to be removed or transported to a higher atmosphere, thereby decreasing the concentration of the UTLS layer. For those boundary layer pollutants which have sources in the stratosphere, such as O_3 and SO_2 (which respectively originate from ultraviolet photolysis and organic sulfide oxidation; Chin and Davis 1995), the STT will be relatively large, accounting for over 40% of the TST. The TST masses of each pollutant within 25 h were sorted from large to small as follows: CO (6.0×10^7 kg), O_3 (2.4×10^7 kg), $PM_{2.5}$ (7.9×10^6 kg), NO_2 (2.2×10^5 kg), and SO_2 (2.7×10^3 kg), within the ~300 km × 300 km domain.

Previous studies have shown that when pollutants are transported to the stratosphere above 380 K, they enter the overworld via the circulation (Holton et al. 1995). Normalizing the transport fluxes of different heights caused by deep convection activities can aid in exploring the height which the upward transport can reach. As the height increases, the upward transport flux decreases rapidly. Of the mass of pollutants transported across the tropopause, only 47% of O_3, 13%

of CO, 14% of SO_2, 34% of NO_2, and 7.2% of $PM_{2.5}$ are transported above 15 km (near 380 K); only 20% of O_3 can be transported above 17 km; and less than 3% of other pollutants remain (Fig. S4). It can be seen that approximately 7.2%–47% of boundary layer pollutants can enter the area above 380 K and affect the global pollution distribution. The remaining pollutants will return to the troposphere through isentropic motion or tropospheric intrusion.

Pierce et al. (2003) observed that the daily average flux of ozone from the stratosphere into troposphere was ~0.22 Tg day^{-1}, exceeding the net production minus loss in the domain (~0.17 Tg day^{-1}) by 0.05 Tg day^{-1}, in the 6600 km × 4500 km domain. Büker et al. (2008) indicated that the total net ozone flux into the troposphere was calculated to be about 0.2 Tg across the 1250 km × 1250 km domain. Hitchman et al. (2004) found that approximately 0.8 Tg day^{-1} of ozone entered the troposphere near the periphery of the convection. Comparing the above-mentioned fluxes with a unified unit of kg km^{-2} day^{-1}, the downward transport flux of ozone from the stratosphere caused by this deep convection event on 21 July was 1–17 times that of previous calculations, while the upward transport flux of ozone from the troposphere was approximately 48 times that of previous calculations. These conclusions indicate that this was a very extreme event which likely transported large amounts of surface pollutants into the stratosphere.

d. *Cross-tropopause transport potential of global deep convection*

Penetrating deep convection, when it occurs over a polluted area, is potentially important for transporting relatively fresh pollution from the boundary layer to the stratosphere. Nonpenetrating deep convection can still eventually transport air masses to the stratosphere via slow radiative driven ascent (Holton et al. 1995; Ploeger et al. 2017), which is believed to be the dominant pathway for air masses traveling upward across the tropopause (Randel et al. 2010). This has the potential to loft aged pollution or longer-lived pollutants. As discussed in the previous sections, and by adopting the Beijing 21 July torrential rainfall event as a case study, it was demonstrated that the cross-tropopause transport flux of polluted compositions may occur, possibly due to even a single deep convection system. Therefore, the question remains as to which regions of the world have stronger transport capacities for deep convection systems. To further elucidate this matter, we have designed a vertical transport potential index, the calculation method of which is as follows:

$$\text{Index} = \text{population} \times \text{mean\_area}, \tag{6}$$

where population represents the number of deep convection systems over April 2014 to March 2018, mean_area represents the average area of each deep convection system (unit: km^2), and all variables in Eq. (6) are treated with the lapse rate tropopause (Z_{LRT}) (WMO 1957). The number of penetrating deep convection and the cross-sectional area were calculated by Ku-band radar precipitation features (KuRPFs), detected by Global Precipitation Measurement (GPM); the penetrating deep convection is defined by precipitation features with 20 dBZ echo-top height greater than Z_{LRT}; and the 5° × 5° dataset used in this study was provided by Nana Liu of Texas A&M University. For more details, see Liu and Liu (2016).

The satellite data showed that, from April 2014 to March 2018, a total of 12 521 penetrating deep convective events occurred worldwide (Fig. 10a), and the cross-sectional area of the ascending air reaching the tropopause was 2.0 × 10^6 km^2 (Fig. 10b). Deep convections occurred mainly on land, and were concentrated in central North America, Europe, central Africa, and Southeast Asia. The area of deep convection was greater in the middle latitudes than in low latitudes. The normalized vertical transport potential index (normalized index = index$_i$/max(index) where i represents the grid point) represents the most frequent deep convective activity, and the largest penetrating area of the tropopause in the world. The regions with the highest index are the northern United States and southern Canada (>0.8), followed by coastal areas of Argentina (0.5–0.8), central Africa, most of Europe, and northern Asia (0.1–0.5), and other regions with indices below 0.1. It is interesting to note that Beijing's corresponding index is 0.26.

The concentration of ozone in the troposphere is much lower than that in the stratosphere. Therefore, our results suggest that that the impact of ozone vertical transport on the UTLS layer is consistent with the transport potential of deep convection. However, for the pollutants that are mainly present in the boundary layer, such as CO, SO_2, and $PM_{2.5}$, their impact on the UTLS layer is related to the transport potential of deep convection, and it is also affected by the surface concentration distribution. If a region features strong deep convection and high pollutant concentration, it is considered that the area is a potential source of pollutants in the UTLS layer. Figures 10d–f respectively illustrate the surface concentration distributions of CO, SO_2, and $PM_{2.5}$. Comparing the deep convective transport potential (Fig. 10c) and pollutant concentration, it can be seen that North America, central Africa, and eastern Asia are potential sources of CO in the UTLS layer; eastern Asia and western Europe are potential sources of SO_2 in the UTLS layer; and central Africa and western Europe are potential sources of $PM_{2.5}$ in the UTLS layer.

This part combines the global deep penetrating convection distribution and pollutants concentration distribution, discusses the cross-tropopause transport potential of boundary layer pollutants in different regions of the world, and proposes several potential pollution source regions. However, these are not the final results. To analyze the global cross-tropopause transport flux, it is necessary to further observe the rising speed of deep convection and the chemical reaction of pollutants in the transportation processes.

4. Conclusions

In the present study, the WRF/CMAQ model was applied to simulate atmospheric processes during the Beijing 21 July torrential rainfall event. The vertical profile changes of pollutant values were determined using satellite and reanalysis data, and the IPR process analysis method was adopted to investigate the factors influencing the value change. Furthermore, the transport flux of pollutants during the

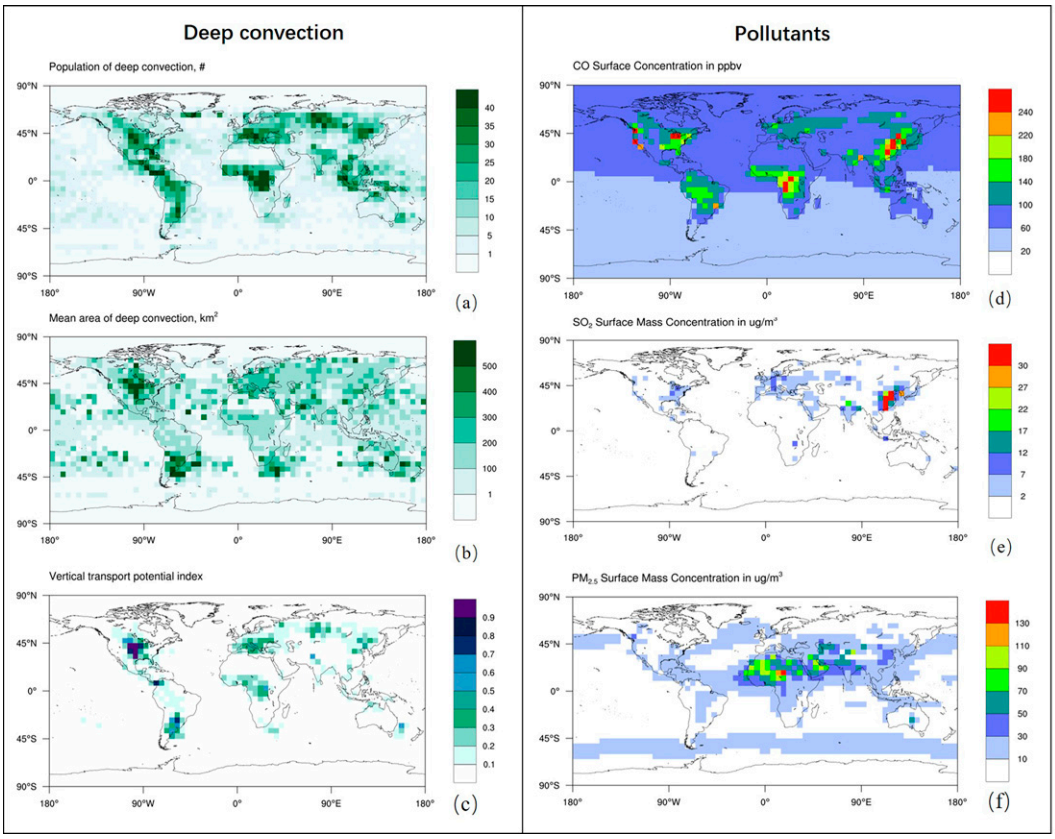

FIG. 10. Distribution of global penetrating deep convection and pollution concentration: (a) population of deep convection, (b) average area of deep convection reaching the tropopause, and (c) normalized vertical transportation potential index at the tropopause, and surface concentrations of (d) CO, (e) SO_2, and (f) $PM_{2.5}$ from April 2014 to March 2018.

event was calculated, and the cross-tropopause transport potential of global deep convection was estimated.

The main conclusions include the following points: First, during the torrential rainfall event (0000 UTC 21 July to 0600 UTC 22 July 2012), a strong updraft occurred, in turn leading to an increase in high-level water vapor and the rise of the tropopause by altering the atmospheric temperature gradient. At the same time, the tropospheric pollutants were transported to the stratosphere. Second, when deep penetrating convection occurred, the O_3 value decreased by 35%, and CO increased by 98% in the UTLS layer. These value changes of O_3 and CO were mainly attributed to atmospheric transport. At lower altitudes (below 4 km), the values of the pollutants decreased due to the removal of precursors by rainfall and reduced photochemical production. Third, the transport fluxes of deep convection to pollutants decreased with increasing altitude, and the respective cross-tropopause transport masses of CO, O_3, $PM_{2.5}$, NO_2, and SO_2 were 6.0×10^7, 2.4×10^7, 7.9×10^6, 2.2×10^5, and 2.7×10^3 kg, within a ~300 km × 300 km domain. The downward stratosphere-to-troposphere flux was smaller than the upward troposphere-to-stratosphere flux, and this deep convection mainly caused a net upward flux of pollutants from the troposphere to the stratosphere. Finally, the estimation of the normalized vertical transport potential index revealed that the northern United States and southern Canada are the regions with the highest potential for tropopause-penetrating deep convection.

In summary, it was observed that deep convection could remove pollutants in the troposphere and improve surface air quality while transporting the surface pollutants into the stratosphere. Penetrating deep convection is universal on a global scale, and there is the possibility of transporting surface pollutants to the stratosphere. Although the number of pollutants transported to the stratosphere by individual deep convection events is limited, the effects of global deep convection on the stratospheric climate cannot be ignored, particularly in midlatitude regions (with frequent deep convection and high pollutant concentration). Therefore, the authors suggest that in the future we attempt to simulate the vertical transport of pollutants by penetrating deep convection through a global-scale model. At the same time, the residence time and transmission path of pollutants after entering the UTLS layer can be analyzed, so as to further elucidate the impact of boundary layer pollutants on the climate of the UTLS layer.

Acknowledgments. This work was supported by the National Nature Science Funds (41425020, 42121004, and

41675031); China Special Fund for Meteorological Research in the Public Interest (GYHY201206015); National Key R&D Program of China (2017YFC0210105 and 2016YFC 0202206); Special Fund Project for Science and Technology Innovation Strategy of Guangdong Province (Grant 2019B1 21205004); and Collaborative Innovation Center of Climate Change, Jiangsu Province, China.

REFERENCES

Büker, M. L., M. H. Hitchman, G. J. Tripoli, R. B. Pierce, E. V. Browell, and J. A. Al-Saadi, 2008: Long-range convective ozone transport during INTEX. *J. Geophys. Res.*, **113**, D14S90, https://doi.org/10.1029/2007JD009345.

Byun, D. W., and J. K. S. Ching, 1999: Science algorithms of the EPA models-3 Community Multiscale Air Quality (CMAQ) modeling system. EPA Rep. EPA/600/R-99/030, 22 pp.

Chen, Z., X. Xie, J. Cai, D. Chen, B. Gao, B. He, N. Cheng, and B. Xu, 2018: Understanding meteorological influences on $PM_{2.5}$ values across China: A temporal and spatial perspective. *Atmos. Chem. Phys.*, **18**, 5343–5358, https://doi.org/10.5194/acp-18-5343-2018.

Chin, M., and D. D. Davis, 1995: A reanalysis of carbonyl sulfide as a source of stratospheric background sulfur aerosol. *J. Geophys. Res.*, **100**, 8993–9005, https://doi.org/10.1029/95JD00275.

Dee, D. P., and Coauthors, 2011: The ERA-Interim reanalysis: Configuration and performance of the data assimilation system. *Quart. J. Roy. Meteor. Soc.*, **137**, 553–597, https://doi.org/10.1002/qj.828.

Dessler, A. E., and S. C. Sherwood, 2004: Effect of convection on the summertime extratropical lower stratosphere. *J. Geophys. Res.*, **109**, D23301, https://doi.org/10.1029/2004JD005209.

Doherty, R. M., D. S. Stevenson, W. J. Collins, and M. G. Sanderson, 2005: Influence of convective transport on tropospheric ozone and its precursors in a chemistry-climate model. *Atmos. Chem. Phys.*, **5**, 3205–3218, https://doi.org/10.5194/acp-5-3205-2005.

Duncan, B. N., S. E. Strahan, Y. Yoshida, S. D. Steenrod, and N. Livesey, 2007: Model study of the cross-tropopause transport of biomass burning pollution. *Atmos. Chem. Phys.*, **7**, 3713–3736, https://doi.org/10.5194/acp-7-3713-2007.

Gettelman, A., and T. Birner, 2007: Insights into tropical tropopause layer processes using global models. *J. Geophys. Res.*, **112**, D23104, https://doi.org/10.1029/2007JD008945.

——, J. R. Holton, and H. Rosenlof, 1997: Mass fluxes of O_3, CH_4, N_2O, and CF_2Cl_2 in the lower stratosphere calculated from observational data. *J. Geophys. Res.*, **102**, 19 149–10 159, https://doi.org/10.1029/97JD01014.

Guo, J., and Coauthors, 2016: The climatology of planetary boundary layer height in China derived from radiosonde and reanalysis data. *Atmos. Chem. Phys.*, **16**, 13 309–13 319, https://doi.org/10.5194/acp-16-13309-2016.

Hitchman, M. H., M. L. Buker, G. J. Tripoli, R. B. Pierce, J. A. Al-Saadi, E. V. Browell, and M. A. Avery, 2004: A modeling study of an East Asian convective complex during March 2001. *J. Geophys. Res.*, **109**, D15S14, https://doi.org/10.1029/2003JD004312.

Holton, J. R, P. H. Haynes, M. E. McIntyre, A. R. Douglass, and B. Rood, 1995: Stratosphere-troposphere exchange. *Rev. Geophys.*, **33**, 403–439, https://doi.org/10.1029/95RG02097.

Hou, X., B. Zhu, D. Fei, and D. Wang, 2015: The impacts of summer monsoons on the ozone budget of the atmospheric boundary layer of the Asia-Pacific region. *Sci. Total Environ.*, **502**, 641–649, https://doi.org/10.1016/j.scitotenv.2014.09.075.

Hsu, J., M. J. Prather, and O. Wild, 2005: Diagnosing the stratosphere-to-troposphere flux of ozone in a chemistry transport model. *J. Geophys. Res.*, **110**, D19305, https://doi.org/10.1029/2005JD006045.

Khodayari, A., F. Vitt, D. Phoenix, and D. J. Wuebbles, 2018: The impact of NOx emissions from lightning on the production of aviation-induced ozone. *Atmos. Environ.*, **187**, 410–416, https://doi.org/10.1016/j.atmosenv.2018.05.057.

Lamarque, J., and Coauthors, 2012: CAM-chem: Description and evaluation of interactive atmospheric chemistry in the Community Earth System Model. *Geosci. Model Dev.*, **5**, 369–411, https://doi.org/10.5194/gmd-5-369-2012.

Lelieveld, J., and P. J. Crutzen, 1994: Role of deep cloud convection in the ozone budget of the troposphere. *Science*, **264**, 1759–1761, https://doi.org/10.1126/science.264.5166.1759.

——, and Coauthors, 2018: The South Asian monsoon—Pollution pump and purifier. *Science*, **361**, 270–273, https://doi.org/10.1126/science.aar2501.

Li, J., Y. Yin, L. Jin, and C. Zhang, 2010: A numerical study of tropical deep convection using WRF Model. *J. Trop. Meteor.*, **16**, 247–254.

Li, Q., and Coauthors, 2005: North American pollution outflow and the trapping of convectively lifted pollution by upper-level anticyclone. *J. Geophys. Res.*, **110**, D10301, https://doi.org/10.1029/2004JD005039.

Liaskos, C. E., D. J. Allen, and K. E. Pickering, 2015: Sensitivity of tropical tropospheric composition to lightning NO_x production as determined by replay simulations with GEOS-5. *J. Geophys. Res. Atmos.*, **120**, 8512–8534, https://doi.org/10.1002/2014JD022987.

Liu, C., and E. J. Zipser, 2005: Global distribution of convection penetrating the tropical tropopause. *Geosci. Model Dev.*, **110**, D23104, https://doi.org/10.1029/2005JD006063.

Liu, N., and C. Liu, 2016: Global distribution of deep convection reaching tropopause in 1 year GPM observations. *J. Geophys. Res. Atmos.*, **121**, 3824–3842, https://doi.org/10.1002/2015JD024430.

——, X. S. Wang, Y. T. Hu, J. Y. Zheng, L. J. Zhong, M. Hu, and Y. H. Zhang, 2012: Numerical simulation and process analysis of PM_{10} pollution over the Pearl River delta in autumn. *China Environ. Sci.*, **32**, 1537–1545.

Lu, X., and Coauthors, 2018: Severe surface ozone pollution in China: A global perspective. *Environ. Sci. Technol. Lett.*, **5**, 487–494, https://doi.org/10.1021/acs.estlett.8b00366.

Mebust, M. R., B. K. Eder, F. S. Binkowski, and S. J. Roselle, 2003: Models-3 Community Multiscale Air Quality (CMAQ) model aerosol component 2. Model evaluation. *J. Geophys. Res. Atmos.*, **108**, 4184, https://doi.org/10.1029/2001jd001410.

Park, M., W. J. Randel, D. E. Kinnison, R. R. Garcia, and W. Choi, 2004: Seasonal variation of methane, water vapor, and nitrogen oxides near the tropopause: Satellite observations and model simulations. *J. Geophys. Res.*, **109**, D03302, https://doi.org/10.1029/2003JD003706.

——, ——, A. Gettelman, S. T. Massie, and J. H. Jiang, 2007: Transport above the Asian summer monsoon anticyclone inferred from Aura Microwave Limb Sounder tracers. *J. Geophys. Res.*, **112**, D16309, https://doi.org/10.1029/2006JD008294.

Pierce, R. B., and Coauthors, 2003: Regional Air Quality Modeling System (RAQMS) predictions of the tropospheric ozone budget over East Asia. *J. Geophys. Res.*, **108**, 8825, https://doi.org/10.1029/2002JD003176.

Ploeger, F., P. Konopka, K. Walker, and M. Riese, 2017: Quantifying pollution transport from the Asian monsoon anticyclone into the lower stratosphere. *Atmos. Chem. Phys.*, **17**, 7055–7066, https://doi.org/10.5194/acp-17-7055-2017.

Randel, W. J., and E. J. Jensen, 2013: Physical processes in the tropical tropopause layer and their roles in a changing climate. *Nat. Geosci.*, **6**, 169–176, https://doi.org/10.1038/ngeo1733.

——, M. Park, L. Emmons, D. Kinnison, P. Bernath, K. A. Walker, C. Boone, and H. Pumphrey, 2010: Asian monsoon transport of pollution to the stratosphere. *Science*, **328**, 611–614, https://doi.org/10.1126/science.1182274.

Sander, R., 2015: Compilation of Henry's law constants (version 4.0) for water as solvent. *Atmos. Chem. Phys.*, **15**, 4399–4981, https://doi.org/10.5194/acp-15-4399-2015.

Solomon, S., J. S. Daniel, R. R. Neely, J.-P. Vernier, E. G. Dutton, and L. W. Thomason, 2011: The persistently variable "background" stratospheric aerosol layer and global climate change. *Science*, **333**, 866–870, https://doi.org/10.1126/science.1206027.

Tang, Q., M. J. Prather, and J. Hsu, 2011: Stratosphere-troposphere exchange ozone flux related to deep convection. *Geophys. Res. Lett.*, **38**, L03806, https://doi.org/10.1029/2010GL046039.

Thompson, A. M., 1994: Convective transport over the central United States and its role in regional CO and ozone budgets. *J. Geophys. Res.*, **99**, 18 703–18 711, https://doi.org/10.1029/94jd01244.

Tian, W., M. Chipperfield, and Q. Huang, 2008: Effects of the Tibetan Plateau on total column ozone distribution. *Tellus*, **60B**, 622–635, https://doi.org/10.1111/j.1600-0889.2008.00338.x.

Vernier, J. P., L. W. Thomason, and J. Kar, 2011: CALIPSO detection of an Asian tropopause aerosol layer. *Geophys. Res. Lett.*, **38**, L07804, https://doi.org/10.1029/2010GL046614.

——, and Coauthors, 2015: Increase in upper tropospheric and lower stratospheric aerosol levels and its potential connection with Asian pollution. *J. Geophys. Res. Atmos.*, **20**, 1608–1619, https://doi.org/10.1002/2014JD022372.

Wang, Y., Y. Zhang, J. Hao, and M. Luo, 2011: Seasonal and spatial variability of surface ozone over China: Contributions from background and domestic pollution. *Atmos. Chem. Phys.*, **11**, 3511–3525, https://doi.org/10.5194/acp-11-3511-2011.

Wedi, N. P., and Coauthors, 2015: The modelling infrastructure of the Integrated Forecasting System: Recent advances and future challenges. ECMWF Tech. Memo. 760, 50, pp.

WMO, 1957: Meteorology—A three-dimensional science: Second session of the Commission for Aerology. *WMO Bull.*, **4**, 134–138.

Yoo, J. M., and Coauthors, 2014: New indices for wet scavenging of air pollutants (O_3, CO, NO_2, SO_2, and PM_{10}) by summertime rain. *Atmos. Environ.*, **82**, 226–237, https://doi.org/10.1016/j.atmosenv.2013.10.022.

Yu, P., and Coauthors, 2017: Efficient transport of tropospheric aerosol into the stratosphere via the Asian summer monsoon anticyclone. *Proc. Natl. Acad. Sci. USA*, **114**, 6972–6977, https://doi.org/10.1073/pnas.1701170114.

Zhao, C., Y. Wang, Q. Yang, R. Fu, D. Cunnold, and Y. Choi, 2010: Impact of East Asian summer monsoon on the air quality over China: View from space. *J. Geophys. Res.*, **115**, D09301, https://doi.org/10.1029/2009JD012745.